**Nacromolecules** 2018, 51, 8821–8832

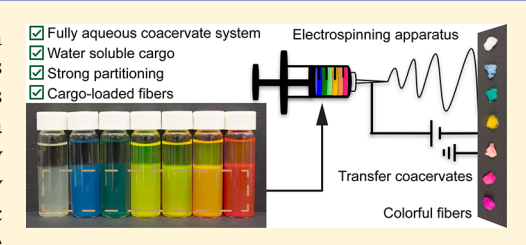
# **Electrospinning Cargo-Containing Polyelectrolyte Complex Fibers:** Correlating Molecular Interactions to Complex Coacervate Phase **Behavior and Fiber Formation**

Xiangxi Meng, Jessica D. Schiffman,\* and Sarah L. Perry\*

Department of Chemical Engineering, University of Massachusetts Amherst, Amherst, Massachusetts 01003, United States

Supporting Information

**ABSTRACT:** We present the first demonstration of the direct encapsulation of cargo into polyelectrolyte complex (PEC) fiber mats. This approach takes advantage of the intrinsic self-assembly characteristics of complex coacervates to simplify the formulation requirements to electrospin fibers containing a high loading and an even distribution of cargo. Two families of structurally similar fluorescent dyes were used as model cargo of varying hydrophobicity and charge and were encapsulated into coacervates of poly(4-styrenesulfonic acid, sodium salt) and poly(diallyldimethylammonium chloride). The



coacervate phase behavior, dye partitioning, and resulting fibers were systematically investigated as a function of dye and salt concentration. Strong partitioning was facilitated by favorable electrostatic and  $\pi-\pi$  interactions but was adversely affected by increased salt. We further identified that dye and salt interactions can be treated as independent control parameters to modulate the properties and electrospinnability of the coacervate precursor solutions. These findings facilitate the use of electrospun PEC fibers in applications related to biomedicine, energy, and separations where cargo-loaded mats are needed.

# 1. INTRODUCTION

Electrospinning enables the fabrication of highly porous mats composed of fibers with large surface area-to-volume ratios that can be easily tailored for a specific application.<sup>1-4</sup> Fiber mats used in advanced medical applications, such as wound dressings, <sup>4–7</sup> tissue engineering scaffolds, <sup>8</sup> and drug delivery platforms, <sup>7,9–12</sup> benefit from having active agents incorporated within the fibers. While a variety of strategies exist to incorporate active agents into electrospun fibers, the methods can be challenging to implement on an industrial scale. For example, core/shell electrospinning requires optimizing the rheology of two fluids, <sup>13–17</sup> whereas layer-by-layer deposition is a discontinuous postprocessing strategy. 9,18,19 Notably, the incorporation of active agents inside fibers oftentimes requires surfactants and toxic organic solvents and results in a low loading of the encapsulated cargo. 20-23 "Greener" methods for electrospinning fiber mats without organic solvents that have a high loading of small molecule cargo are needed.

Recently, we demonstrated that polymer-based complex coacervates could be electrospun into polyelectrolyte complex (PEC) fibers using an entirely water-based methodology.<sup>2</sup> Complex coacervation is an associative liquid-liquid phase separation that occurs due to the electrostatic and entropic interactions between oppositely charged macro-ions in water.<sup>25-29</sup> The self-assembly, phase behavior, and properties of the resulting dense, polymer-rich coacervate phase can be controlled by proper parameter selection, including the relative concentration of the charged polymers, polymer chain length, chemistry of the charged species, ionic strength, and pH.<sup>28,30-'34</sup> Our first report demonstrated that the polymerrich coacervate phase could be directly used as a precursor

solution and electrospun into PEC fiber mats.<sup>24</sup> One interesting consequence of the strong electrostatic attractions driving complexation is the excellent stability of PEC fibers against both heat and dissolution in a broad range of organic solvents and pH conditions.<sup>24</sup>

A critical observation in our initial work was the interplay between coacervate phase behavior and the electrospinnability of the resulting materials. While complex coacervates have a tremendous history of applications related to the encapsulation of both hydrophobic and hydrophilic cargo, 35-45 there have been few systematic studies that investigate how the molecular properties of small molecules drive encapsulation and/or modulate the phase behavior and properties of the coacervate itself.46 Recent work by Zacharia and co-workers demonstrated the importance of charge and hydrophobicity in driving the partitioning of small molecule dyes into various polymer-based coacervates. 47,48 However, it remains unclear how subtle variations in the chemistry of the cargo molecules would modulate encapsulation or how the incorporation of molecules would affect the electrospinnability of the resulting coacervates.

Here, we utilized a panel of six water-soluble fluorescent dyes (Figure 1) as model cargo to systematically examine how changes in the chemical structure and properties of structurally similar small molecules would affect their encapsulation into complex coacervates formed from poly(4-styrenesulfonic acid, sodium salt) (PSS) and poly(diallyldimethylammonium chloride) (PDADMAC) in potassium bromide (KBr)

Received: August 8, 2018 Revised: October 16, 2018 Published: October 29, 2018



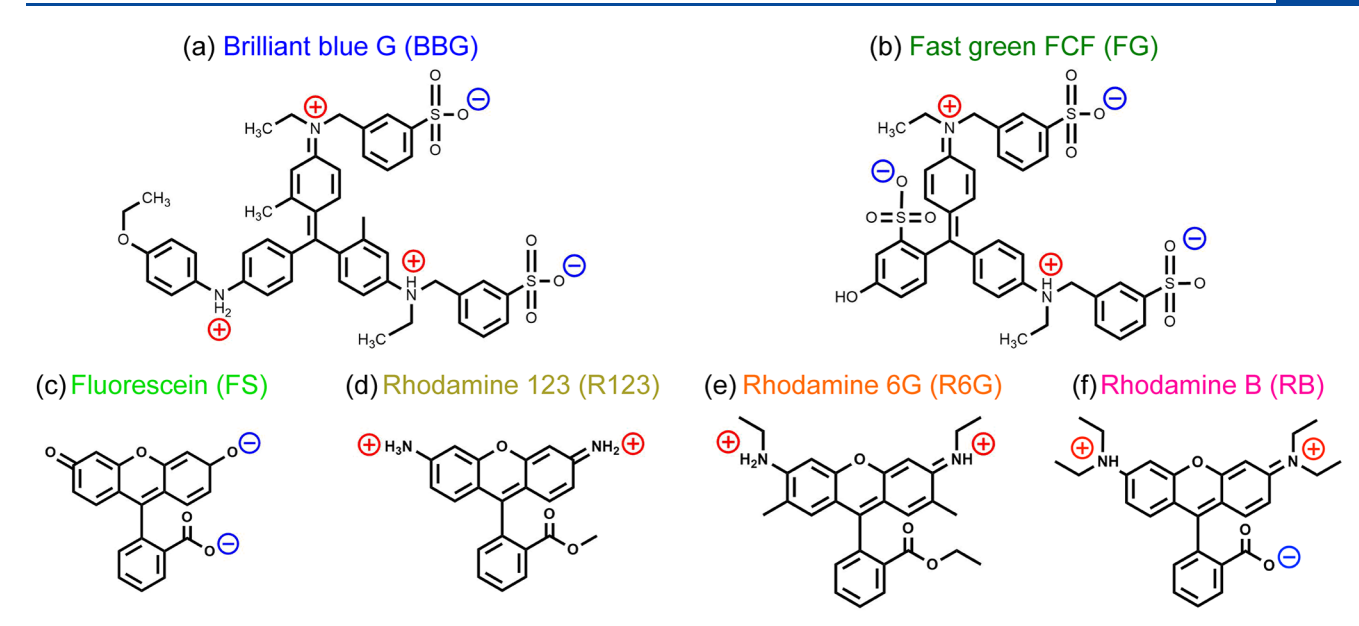


Figure 1. Chemical structures of (a) brilliant blue G (BBG), (b) fast green FCF (FG), (c) fluorescein sodium salt (FS), (d) rhodamine 123 (R123), (e) rhodamine 6G (R6G), and (f) rhodamine B (RB). Charges are labeled based on the ionized form of the dyes in a pH = 7.2 solution. Counterions have been left off for simplicity. A detailed comparison between dyes is provided in Table S1.



Figure 2. Schematic of the process used to electrospin the coacervate phase into polyelectrolyte complex (PEC) fiber mats. Dye-free complex coacervates composed of poly(4-styrenesulfonic acid, sodium salt) (PSS), poly(diallyldimethylammonium chloride) (PDADMAC), and potassium bromide (KBr) in water and coacervates containing brilliant blue G (BBG), fast green FCF (FG), fluorescein sodium salt (FS), rhodamine 123 (R123), rhodamine 6G (R6G), and rhodamine B (RB) were electrospun. The polymer-rich coacervate phase was used as the electrospinning precursor solution. The SEM and fluorescence micrographs show FS-containing PEC fibers.

solutions. We further explored how the presence of the various cargo molecules altered the phase behavior, properties, and subsequent electrospinnability of the resulting coacervates (Figure 2).

# 2. EXPERIMENTAL SECTION

2.1. Materials. Poly(4-styrenesulfonic acid, sodium salt) (PSS, AkzoNobel, VERSA TL130, 15 wt % solution in water, ca. 332 000 g/ mol,  $N \sim 1600$ , PDI  $\sim 1.08$ ). The molecular weight and PDI of PSS were characterized by aqueous gel permeation chromatography (GPC/SEC-MALS Agilent Technologies, Santa Clara, CA) using a TSKgel G3000SWxl column with a mobile phase of 20/80 v/v mixture of 0.1 M sodium nitrate (NaNO<sub>3</sub>, ACS grade, Sigma-Aldrich, St. Louis, MO) and acetonitrile (C2H3N, ACS grade, Fisher Scientific, Fair Lawn, NJ). PSS was filtered using a 0.22  $\mu$ m pore size filter (EMD Millipore) prior to use. Poly(diallyldimethylammonium chloride) (PDADMAC, Hychem, Hyperfloc CP 626, 20 wt % solution in water, ca. 350 000–400 000 g/mol,  $N \sim 2470$ ) was used as received. Brilliant blue G (BBG, 854.02 g/mol), fast green FCF (FG, 808.86 g/mol), fluorescein sodium salt (FS, 376.27 g/mol), rhodamine 123 (R123, 380.82 g/mol), rhodamine 6G (R6G, 479.02 g/mol), and rhodamine B (RB, 479.02 g/mol) were ACS grade and used as received from Sigma-Aldrich. ACS grade potassium bromide (KBr), hydrochloric acid (HCl), and sodium hydroxide (NaOH) were used as received from Fisher Scientific. Deionized (DI)

water was obtained from a Milli-Q water purification system (resistivity of 18.2 M $\Omega$  cm, Millipore).

2.2. Preparation of Complex Coacervates. PSS and PDADMAC aqueous stock solutions were prepared gravimetrically at 0.5 M on a monomer basis and adjusted to pH 7.2 with a few drops of concentrated HCl or NaOH. Dye was first mixed with an 0.5 M PSS stock solution to make concentrated dye-PSS stock solutions. Dye-containing coacervates were prepared at a total volume of 1.5 mL in microcentrifuge tubes (Fisherbrand 2.0 mL Graduated Natural, Fisher Scientific) for dye concentration measurements and at a total volume of 10 mL in graduated round-bottom tubes (14 mL, Fisher Scientific) for coacervate volume measurements. To prepare dyecontaining coacervates, solid KBr, dye-PSS solution, PSS solution, and PDADMAC solution were sequentially added to a clean, dry container and vortexed for 30 s after each addition to facilitate mixing. Coacervate samples were all prepared at a 1:1 ratio of PSS:PDADMAC, on a monomer basis, and the total PSS and PDADMAC monomer concentration in the final sample was 0.5 M. All samples used for concentration measurements were made in triplicate. Coacervate samples were mixed overnight on a rotator (Arma-Rotator A-1, Elmeco Engineering, Gaithersburg, MD) at 20 rpm until equilibrated before being centrifuged to coalescence the dense coacervate phase. Small-scale samples were centrifuged at 17g for 10 min (Sorvall Legend Micro 17 Centrifuge, Thermo Fisher Scientific), while large-scale samples were centrifuged at 2300g for 10 min (Sorvall ST 16R Centrifuge, Thermo Fisher Scientific). The only

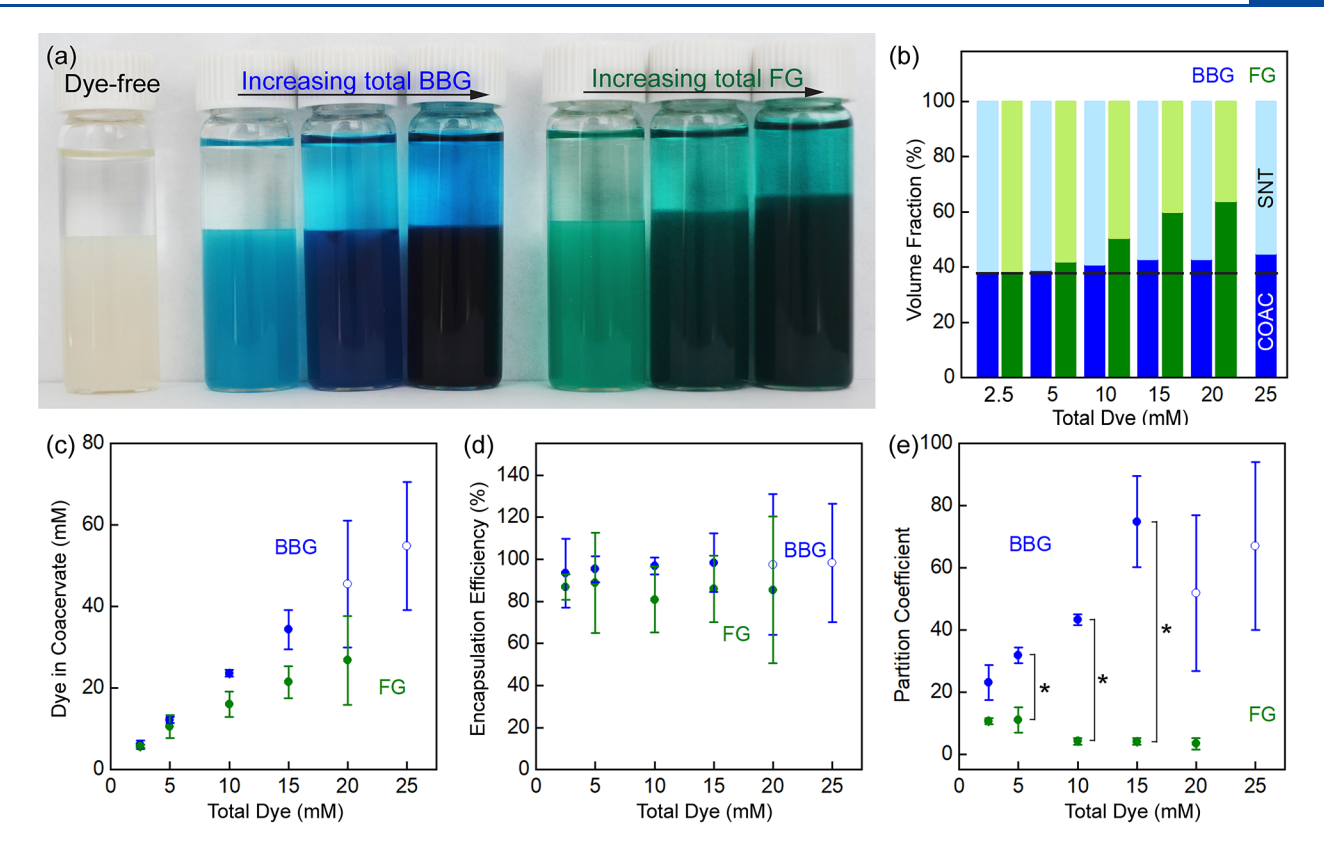


Figure 3. (a) Digital photographs of a dye-free PSS/PDADMAC coacervate sample alongside samples containing increasing amounts of BBG and FG (0.03–0.15 mM dye). (b) The volume fraction of the coacervate (COAC) and supernatant (SNT) phases as a function of increasing dye concentration. The solid back line indicates the volume of the two phases for a dye-free coacervate. Plots of (c) dye concentration in the coacervate, (d) encapsulation efficiency, and (e) the partition coefficient (coacervate/supernatant) as a function of increasing dye concentration. (c–e) Open circles (at or above 20 mM BBG) indicate the presence of precipitated polymer/dye aggregates. All samples were prepared with 0.5 M PSS/PDADMAC, on a monomer basis, in 1.6 M total KBr. An asterisk (\*) denotes p < 0.05 between BBG and FG samples, and error bars denote standard deviation.

exception to this procedure were the highly concentrated FG-containing samples (20 and 25 mM), which were left at room temperature to settle for 90 days to ensure phase separation. Samples prepared for visualization and digital imaging were prepared at a concentration of  $\sim 0.03-0.15$  mM BBG and FG and  $\sim 0.05$  mM FS, R123, R6G, and RB (Figures 2, 3, and 5).

2.3. Determination of Dye Concentration. The volumes of both the supernatant and the coacervate phase were directly read from the graduation marks on the round-bottom tubes following centrifugation. The concentration of dye in the supernatant in each sample was determined by extracting 4-10  $\mu$ L of solution, followed by dilution using dye-free supernatant in a disposable cuvette (1.5 mL, polystyrene, Fisher Scientific). Samples were analyzed using an ultraviolet-visible scanning spectrophotometer 10S (UV/vis, Genesys, Thermo Scientific). Calibration curves were constructed using the peak absorbance wavelength for each dye (Table S2). The concentration of dye in the coacervate phase was calculated via conservation of mass based on the experimentally determined concentration of dye in the supernatant and the volume of the coacervate and supernatant phases. Dye-free supernatant was obtained from a sample prepared at a total monomer concentration of 0.5 M PSS/PDADMAC in 1.6 M KBr, unless otherwise specified.

Changes to the UV/vis spectra for the various dyes in the presence of coacervate components were characterized using solutions of 0.02 mM BBG and FG dissolved in DI water, 1.6 M KBr solution, 10 mM PSS and 10 mM PDADMAC, and dye-free supernatant. Analogous experiments were performed for 0.03 mM FS, R123, R6G, and RB in both DI water and dye-free supernatant. The effect of increasing dye concentration on the observed spectra was studied using samples of 0.10, 0.25, and 0.50 mM BBG and FG in 10 mM PSS and 1.6 M KBr

solution, respectively. For display purposes, the maximum peak absorbance was used as a reference point to normalize the absorbance spectra of each dye (Figures 4 and 5).

The encapsulation efficiency was defined as the fraction of dye present in the coacervate phase, while the partition coefficient was defined as the dye concentration ratio between the coacervate phase and the supernatant phase. 47–49 We also calculated the number of monomers per dye molecule in the coacervate phase as an indication of how interactions between polymer and dye might change as a function of concentration or solution conditions. These calculations assumed that 99% of the polymer present in the entire sample was localized to the coacervate phase. 50

2.4. Electrospinning of Polyelectrolyte Complex (PEC) Fibers. Coacervates were loaded into a 5 mL syringe (Henke Sass Wolf, Norm-Ject Luer Lock) capped with a PrecisionGlide 22 gauge needle (Becton, Dickinson & Co., Franklin Lakes, NJ). The syringe was secured to a PHD Ultra syringe pump (Harvard Apparatus, Plymouth Meeting, PA). Alligator clips were used to connect the positive and negative anodes of a high-voltage supply (Gamma High Voltage Research Inc., Ormond Beach, FL) to the needle and a copper plate wrapped in aluminum foil, respectively.<sup>51</sup> Unless otherwise specified, the coacervate solution was advanced at a constant rate of 1.0 mL/h, the needle-to-collector separation distance was set to 20 cm, and an applied voltage of 14 kV was used. The electrospinning apparatus was housed in an environmental chamber (CleaTech, Santa Ana, CA) maintained at temperature of 24  $\pm$  1 °C and a relative humidity of 28-31% using a desiccant unit (Drierite, Xenia, OH).

2.5. Characterization of Polyelectrolyte Complex (PEC) Fibers. Fiber morphology was examined using a scanning electron

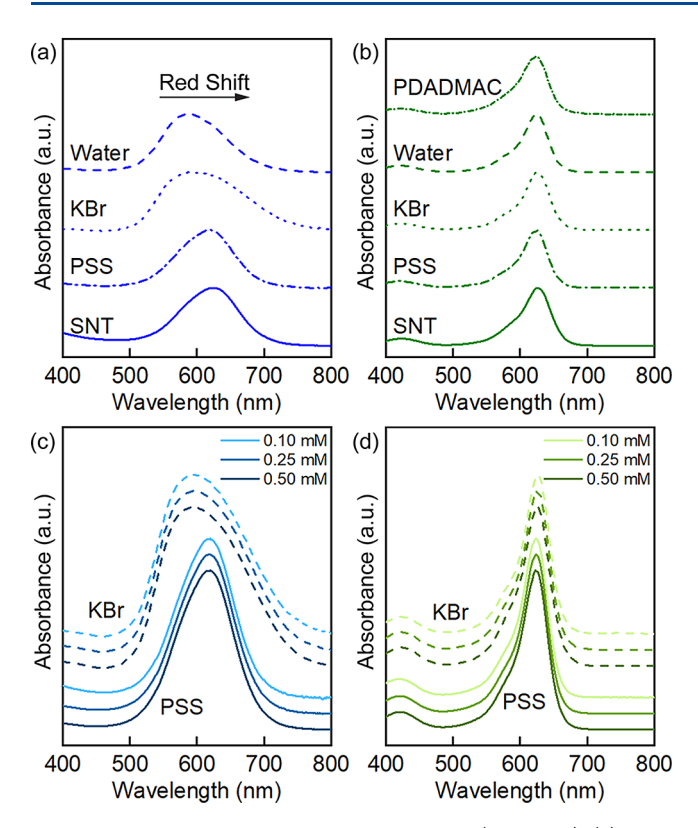


**Figure 4.** UV/vis absorbance spectra for dilute (0.02 mM) (a) BBG and (b) FG in DI water, 1.6 M KBr, 10 mM PSS, 10 mM PDADMAC, and dye-free supernatant. BBG could not be fully dissolved in 10 mM PDADMAC solution. UV/vis absorbance spectra for 0.10, 0.25, and 0.50 mM of (c) BBG and (d) FG in 10 mM PSS solutions in 1.6 M KBr.

microscope (SEM, FEI-Magellan 400). SEM samples were sputter coated for 120 s with gold (Cressington high-resolution ion beam coater model 108). Fiber diameter was determined using ImageJ 1.80 software (National Institutes of Health, Bethesda, MD) to measure 250 fibers from five or more high-resolution SEM micrographs. A Zeiss Axiovert four-laser spinning disc confocal microscope (20× magnification, Oberkochen, Germany) was used to collect bright-field and fluorescence images, Ex/Em 488/509 nm for BBG, 353/465 nm for FG, 495/519 nm for FS, 507/529 nm for R123, 530/552 nm for R6G, and 543/565 nm for RB. A digital single lens reflex (Nikon D5200, Melville, NY) camera with an AF-S NIKKOR 18–35 mm 1:3.5–5.6G lens was used to photograph the PEC fibers.

Attenuated total reflectance Fourier transform infrared spectrometry (ATR-FTIR, Platinum ATR, Bruker Alpha, Billerica, MA) was used to verify the presence of PSS, PDADMAC, BBG, and FG in the PEC fibers. Lyophilized (Labconco, FreeZone Plus 2.5 Liter Cascade Console Freeze-Dry System, Kansas City, MO) PSS and PDADMAC polymers, PEC fibers, as-received BBG and FG, and the BBG- and FG-containing PEC fibers were examined. Coacervate samples were prepared using 0.5 M PSS/PDADMAC in 1.5 M KBr and both the presence and absence of 15 mM total dye concentration. Electrospinning conditions were 1 mL/h, 14 kV, and 20 cm.

**2.6. Statistical Analysis.** Statistical analysis was performed using an unpaired, two-tailed Student's t test. An asterisk (\*) denotes p < 0.05 between samples.

### 3. RESULTS AND DISCUSSION

The goal of this work was to establish a rational framework for (i) understanding the incorporation of small water-soluble molecules (i.e., fluorescent dyes) into complex coacervates, (ii) determining how cargo encapsulation affects the phase

behavior of the coacervates, and (iii) unveiling whether cargo encapsulation influences the electrospinnability of polyelectrolyte complex (PEC) fibers. While previous reports have investigated the encapsulation of dyes into liquid complex coacervates, <sup>47–49,52</sup> much of this work has compared the encapsulation of dyes with vastly different properties (i.e., charged vs neutral) <sup>47–49</sup> and/or significant differences in chemical structure. <sup>47–49,52</sup> Here, our goal was to elucidate how subtle chemical differences between dye molecules can modulate the encapsulation of dye into complex coacervates and the subsequent electrospun fibers using PSS/PDADMAC and KBr as a model system.

3.1. Encapsulation of BBG and FG as a Function of Dye Chemistry and Concentration. To begin with, we examined the encapsulation of increasing amounts of two relatively large fluorescent dyes that have similar chemical structures: brilliant blue G (BBG) and fast green FCF (FG) (Figure 1a,b and Table S1). We observed strong partitioning of both dyes into the polymer-rich coacervate phase and an increase in dye concentration within the coacervate phase when the overall dye loading was increased (Figure 3c). This result was consistent with previous reports, which suggested that relatively hydrophobic polymers favor the uptake of hydrophobic dyes. 47,49 Interestingly, very high levels of encapsulation efficiency were demonstrated with no significant variation over the range of concentrations examined for both dyes (~95%, Figure 3d); however, dramatically different partitioning of the dyes into the coacervate phase was observed as a function of dye loading (Figure 3e). We observed a significant increase in the partition coefficient of BBG with increasing dye concentration, while the partitioning of FG decreased over the same range.

At first glance, these two results appear to be inconsistent. How could an increase in dye concentration lead to different partitioning behaviors, while a similar level of encapsulation efficiency was maintained? Such a result would be physically impossible if the volume of the two phases remained constant. However, while increasing amounts of both dyes led to an increase in the volume of the coacervate phase, these changes were much more dramatic for the case of FG (Figure 3b,e). Thus, the encapsulation data for FG indicate that the same overall fraction of total dye was encapsulated into the coacervate phase, while the larger coacervate volume resulted in a relatively lower dye concentration and, thus, a decrease in the partition coefficient with increasing dye load.

While the observed changes in coacervate volume explain the numerical differences between partitioning and encapsulation efficiency, the question remains as to why the two dyes partitioned differently. BBG and FG have a similar molecular framework, with BBG having a higher total molecular weight. This difference in hydrophobicity based on molecular size could explain why BBG partitions more strongly into the coacervate environment, yet it does not justify the enhanced swelling of the coacervate phase and the decrease in partition coefficient for FG. From an electrostatics perspective, the two dyes have the same total number of charged groups, with BBG having a net charge of +1 and FG having a net charge of -1. On its own, electrostatics also failed to explain why the two dyes would partition differently, as the total contribution to the ionic strength of the solution was the same for BBG and FG. Instead, we consider how combinations of more specific interactions could lead to the observed partitioning behavior.

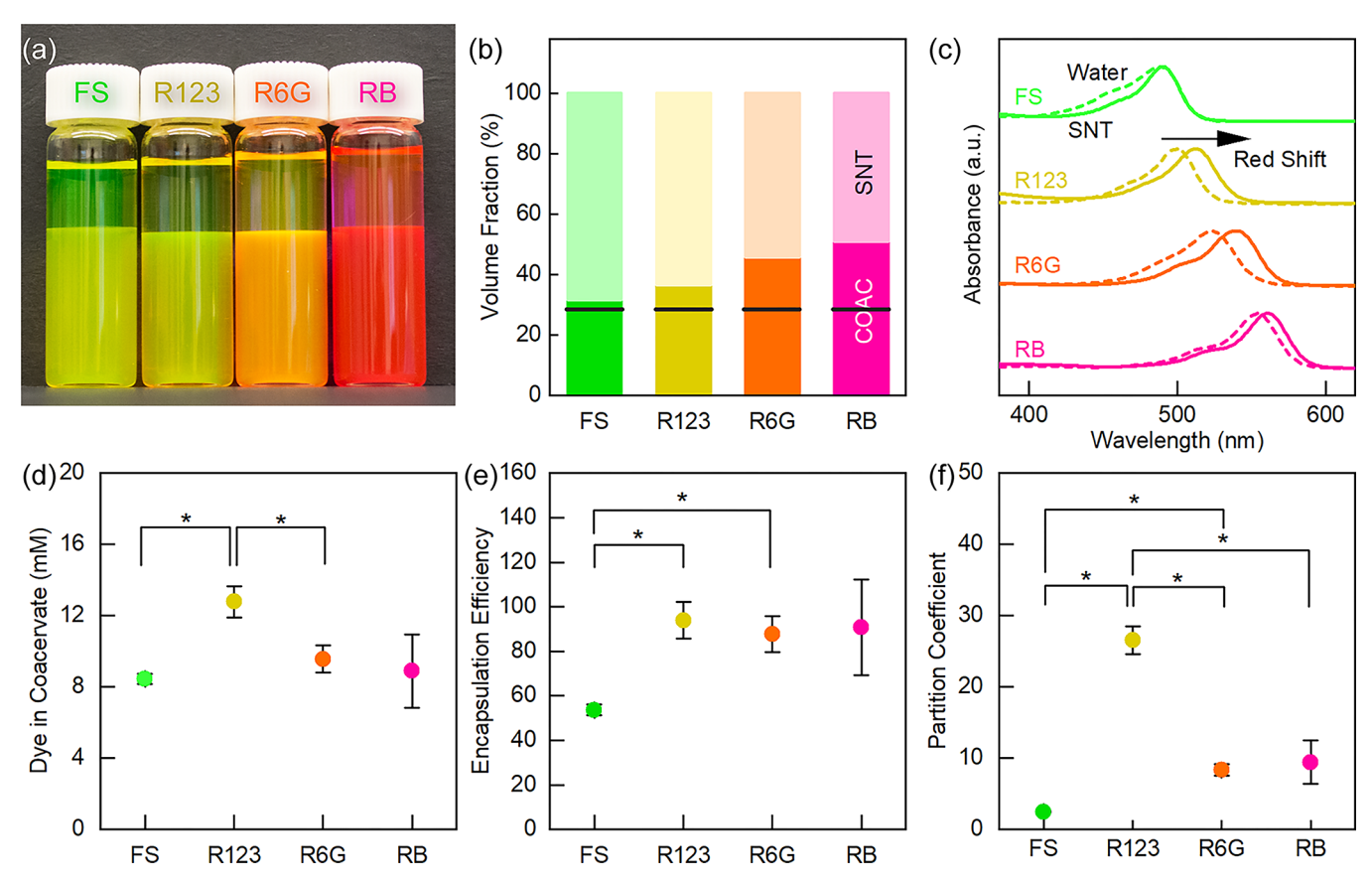


**Figure 5.** (a) Digital photograph of PSS/PDADMAC coacervate samples containing 0.05 mM FS, R123, R6G, and RB. (b) Volume fraction of the coacervate (COAC) and supernatant (SNT) phases in the presence of dyes. The solid black line indicates the volume of the two phases for a dye-free coacervate. (c) UV/vis absorbance spectra for dyes (0.03 mM) in DI water and dye-free supernatant. Plots of the (d) dye concentration in the coacervate, (e) encapsulation efficiency, and (f) the partition coefficient (coacervate/supernatant) for dyes. All samples were prepared with 0.5 M PSS/PDADMAC, on a monomer basis, in 1.5 M total KBr. An asterisk (\*) denotes p < 0.05 between samples, and error bars denote standard deviation.

By their nature, organic dyes are composed of highly conjugated networks of carbon atoms that can form attractive  $\pi$ - $\pi$  interactions with the styrene functionality on PSS. UV/vis spectra showed a strong red-shift in the maximum absorbance peak for BBG in the presence of PSS, characteristic of Jaggregation due to  $\pi$ - $\pi$  interactions, while no such shifts were observed for FG (Figure 4). On the basis of this observation, we conclude that the net positive overall charge on BBG enabled both electrostatic and  $\pi$ - $\pi$  stacking interactions with the negatively charged PSS, while the negative charge on FG prevented such binding. Our data agree with previous reports that there are strong  $\pi - \pi$  interactions between a positively charged methylene blue dye and PSS47,49 and suggest a pathway for increased dye partitioning at higher loading based on  $\pi - \pi$  stacking of dyes with minimal swelling of the coacervate. In contrast, the electrostatic repulsion between FG and PSS leads to larger excluded volume effects, which drives swelling of the coacervate phase and an increased water content. This conclusion is further supported by comparing the ratio of monomer units present in the coacervate phase to the number of dye molecules (Figure S1). Nearly identical trends were observed for BBG and FG, suggesting that any differences in the volume of the coacervate between these two dyes must result from excluded volume differences due to the way that the dyes interact with the polymers rather than swelling due to differences in the number of dye molecules present.

# **3.2. Encapsulation of Fluorescein and Rhodamine Dyes.** We next considered a larger series of chemically similar

**Dyes.** We next considered a larger series of chemically similar fluorescent dyes to examine the effect of more subtle molecular differences on coacervation and dye encapsulation. To this end, we selected a family of fluorescent dyes: fluorescein sodium salt (FS), rhodamine 123 (R123), rhodamine 6G (R6G), and rhodamine B (RB) (Figure 1c-f and Table S1). All three of the rhodamine dyes carry a net positive charge, as in the case of BBG, but incorporate different alkyl moieties. In contrast, FS has a net charge of -2. Based on our hypothesis from the results with BBG and FG, the negatively charged FS should not interact with the PSS and thus should partition more weakly into the coacervate phase than the rhodamine dyes. However, it is not obvious how the subtle structural nuances between the rhodamine dyes would affect uptake and partitioning, as both steric and hydrophobic arguments could be invoked.

Experiments that investigated the loading of rhodamine or FS dye (5 mM total) into PSS/PDADMAC coacervates in 1.5 M KBr showed significant differences in the ways in which the dyes partitioned into the coacervate phase and the extent to which the volume of the coacervate phase was affected by the presence of the dyes (Figure 5). Uniformly, the rhodamine dyes exhibited a higher encapsulation efficiency (~90%) than FS (54%), which showed the lowest efficiency of any of the dyes considered in this study (Figure 5e). However, the measured concentration of dye in the coacervate phase was

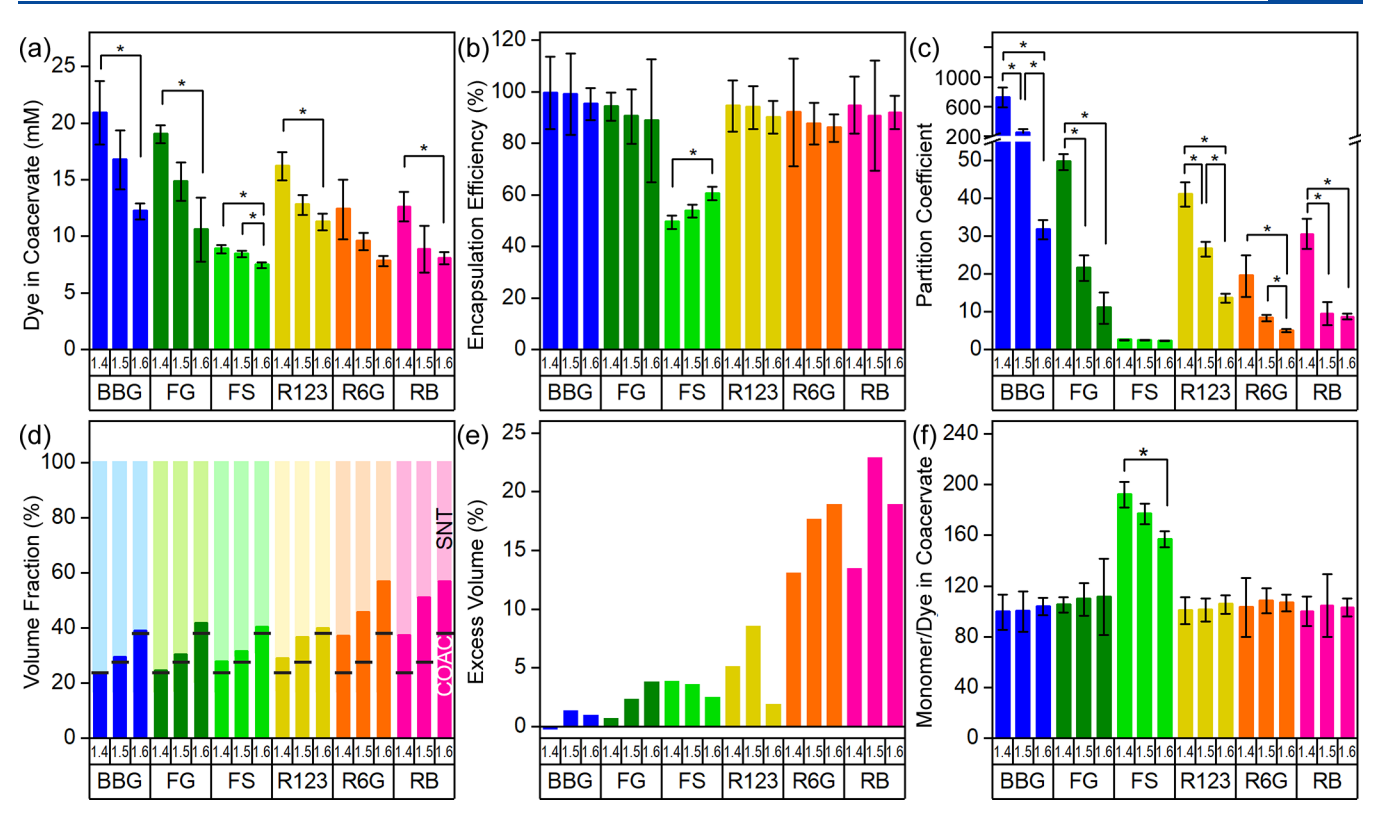


**Figure 6.** Plots of (a) dye concentration in the coacervate, (b) encapsulation efficiency, and (c) the partition coefficient (coacervate/supernatant) and (d) the volume fraction of the coacervate (COAC) and supernatant (SNT) phases in the presence of dyes as a function of KBr concentration. The solid back line indicates the volume of the two phases for a dye-free coacervate. (e) The excess volume of the coacervate phase in the presence of dye compared to that of the dye-free coacervate as a function of the as-prepared KBr concentration. (f) The number of PSS and PDADMAC monomers per dye present in the coacervate. All samples were prepared with 5 mM total dye concentration in 0.5 M PSS/PDADMAC, on a monomer basis. An asterisk (\*) denotes p < 0.05 between samples, and error bars denote standard deviation.

only statistically different for R123 (Figure 5d). Converting from concentration to partitioning, we observed that the partition coefficient of the dyes between the coacervate and supernatant (Figure 5f) was a combinatorial outcome of the encapsulation efficiency and the degree of swelling observed for the coacervate phase (Figure 5b), as was observed in the case of BBG and FG. Interestingly, FS incorporation resulted in minimal swelling of the coacervate, which differed from the outcome observed for FG, whereas more significant swelling was observed for the strongly partitioning R123, R6G, and RB.

While the low encapsulation efficiency of the negatively charged FS was expected based on our results from the BBG and FG experiments, we utilized UV/vis spectroscopy to check for the presence of attractive  $\pi-\pi$  interactions between PSS and the various dyes (Figure 5c). We observed a negligible shift in the peak absorbance for FS but a significant red-shift for all three of the rhodamine dyes, confirming that attractive electrostatic interactions were a prerequisite to enable  $\pi-\pi$  stacking between the dyes and PSS. The combination of repulsive electrostatics and the lack of  $\pi-\pi$  interactions for FS resulted in a very low dye concentration in the coacervate phase and therefore less significant swelling of the coacervate phase compared to other dyes.

Interestingly, despite the strong red-shifting of all three positively charged rhodamine dyes, we observed significant differences in dye partitioning and swelling of the coacervate phase. R123 had the strongest partitioning and the lowest swelling, suggesting the closest interaction between the dye and polymer. We hypothesize that the increased alkylation of

the amine groups on R6G and RB would cause steric hindrance that decreased the effectiveness of the attractive  $\pi$ – $\pi$  interactions, while the additional carboxylate group in RB decreased the electrostatic attraction between, resulting in more significant excluded volume effects. Additionally, we observed a broadening of the absorbance peak for R6G, which suggests that the dye exists in a larger distribution of local electronic environments. Details of peak shifts for all dyes in this study are tabulated in Table S2.

**3.3.** Dye Encapsulation as a Function of Salt Concentration. Thus far, our results have demonstrated that small molecule cargo can have dramatic effects on the coacervate matrix. For example, the coacervate can swell significantly upon dye incorporation. For dye-free coacervate systems, similar swelling has been known known to occur in the presence of increasing salt due to osmotic pressure effects. <sup>26,28,29,53-60</sup> In particular, raising the salt concentration from 1.4 to 1.5 M KBr and from 1.5 to 1.6 M KBr resulted in a 4% and 10% increase in the coacervate volume fraction, respectively (Figure 6d). Therefore, we also examined the interplay between dye encapsulation, partitioning, and coacervate swelling as a function of salt concentration.

Across all dyes, regardless of their size, charge, or the details of the chemistry, we observed a significant decrease in both the concentration of dye present in the coacervate phase and the partitioning of dye into the coacervate phase as the salt concentration increased from 1.4 to 1.6 M KBr (Figure 6a). However, varying the salt concentration did not significantly affect the encapsulation efficiency for any of the dyes, with the

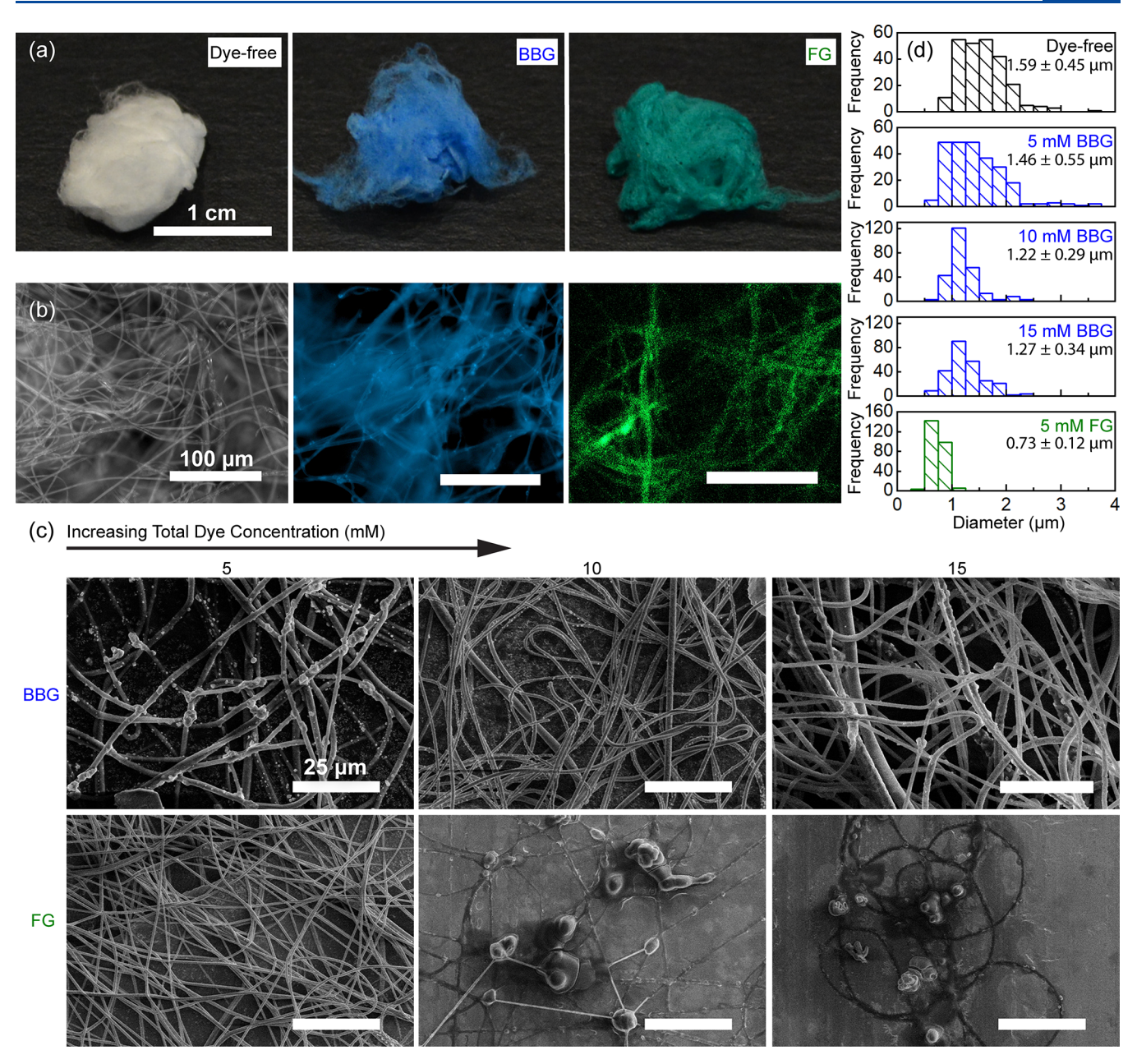


**Figure 7.** (a) Digital photographs and (b) bright-field and fluorescence micrographs of dye-free PSS/PDADMAC PEC fibers (left), BBG-containing PEC fiber (middle), and FG-containing PEC fiber (right). (c) SEM micrographs of as-spun BBG- and FG-containing PEC fibers as a function of dye concentration. Dye-free PEC fibers are shown in Figure S2. (d) Fiber diameter distribution for dye-free, BBG-containing PEC fiber, and FG-containing PEC fiber as a function of dye concentration. The average fiber diameter and standard deviation are indicated, n = 250. All fibers were electrospun from 0.5 M PSS/PDADMAC, on a monomer basis, in 1.6 M KBr. Panels (a) and (b) were electrospun from coacervates containing 5 mM overall dye concentration. The electrospinning conditions used were 1 mL/h, 14 kV, and 20 cm, except for the 10 mM (1.25 mL/h, 18 kV) and 15 mM (1.25 mL/h, 22 kV) FG-containing samples.

noted exception of FS, which showed an increase in encapsulation efficiency with increasing salt concentration (Figure 6b). These data suggest that the combination of increased coacervate volume and decreased dye concentration allowed for the high level of encapsulation efficiency in parallel with decreases in dye partitioning. A summary of the partitioning results for the dyes used in this study is available in Table S3.

Because of the complex interplay between concentration, coacervate swelling, and partitioning, we calculated the number of monomer units per dye molecule present in the coacervate phase as a function of salt concentration. Interestingly, we

obtained a relatively constant value of  $\sim 105$  monomers per dye molecule for all of the dye and salt conditions tested, with the exception of FS (Figure 6f). These results suggest that for many systems increased salt can be treated as an independent control parameter to modulate the polymer concentration and viscosity of the coacervate by enhancing swelling and that the salt does not compete with dye molecules for binding sites along the polymers.

While quantitative and systematic studies that investigate the dye loading and partitioning of cargo in coacervates are scarce in the literature, Zhao et al. described a decrease in the encapsulation of a charged dye (methylene blue) with

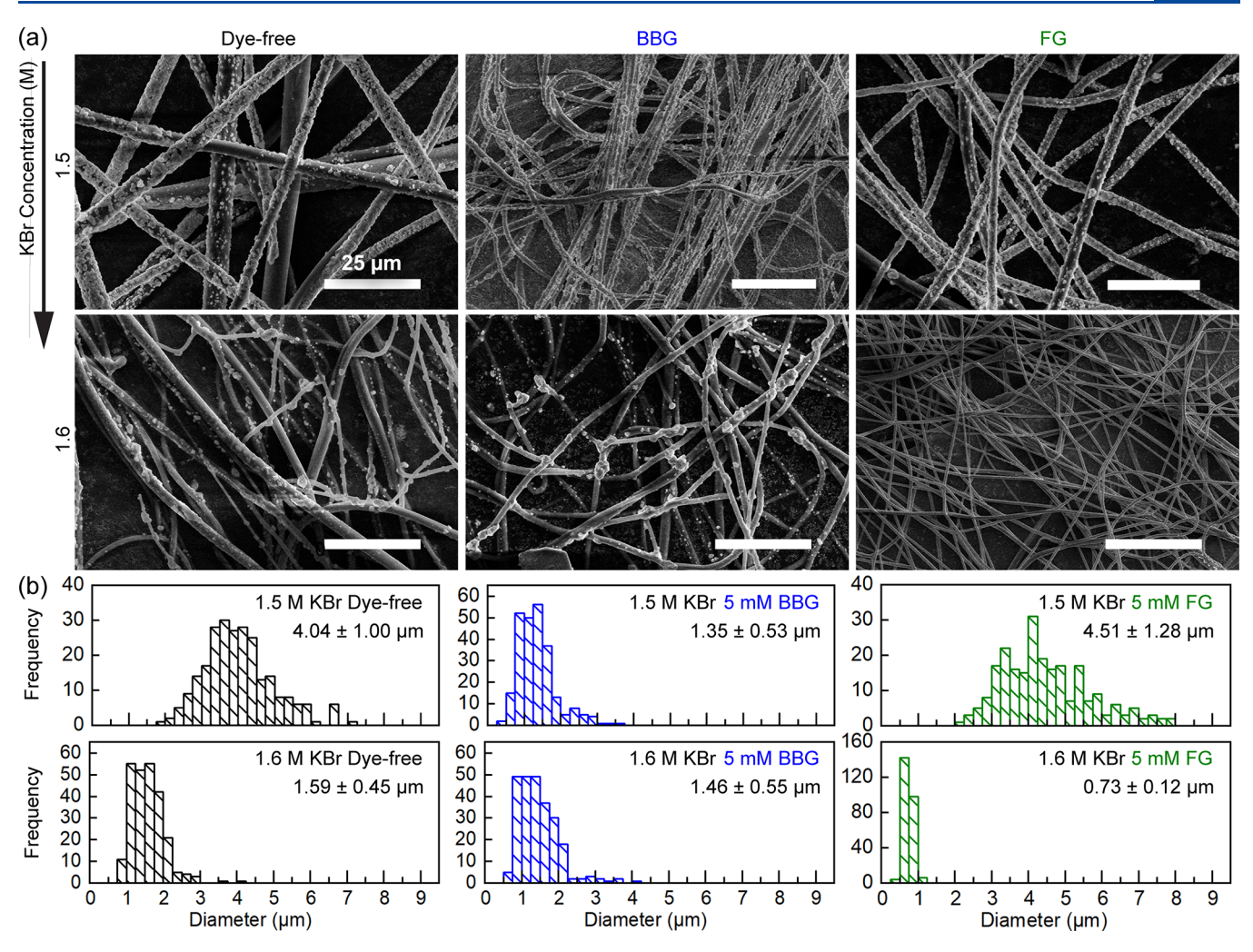


**Figure 8.** (a) SEM micrographs and (b) fiber diameter distributions of dye-free, BBG-, and FG-containing PEC fibers as a function of KBr concentration. The average fiber diameter and standard deviation are indicated, n = 250. All fibers were electrospun from 0.5 M PSS/PDADMAC, on a monomer basis, in 1.5 and 1.6 M KBr in the absence or presence of 5 mM total BBG and FG, respectively. Electrospinning conditions used were 1 mL/h, 14 kV, and 20 cm.

increasing salt concentration.  $^{47}$  Charge screening arguments as well as shifts in the degree of ionization of the polymer were used to explain this result.  $^{48}$  However, the salt concentration in our system is an order of magnitude higher than the previous reports (1.4–1.6 M vs 0–0.2 M), such that the addition of salt would be expected to have a minimal impact on charge screening effects. Instead, our data on the monomer/dye ratio suggest that the observed impact of salt concentration on dye uptake is a consequence of coacervate swelling (Figure 6f and Figure S1).

Both salt and dye have been shown to significantly swell the coacervate phase. Figure 6e quantifies the percent change, or excess volume of the coacervate phase, relative to the dye-free case as a function of salt concentration. In general, we observed volcano-like behavior with a maximum in the excess volume occurring at intermediate salt concentrations for most of the dyes (1.5 M KBr). While a maximum was not observed for FG, FS, or R6G, the data suggest that such a peak might be absent due to the lack of attractive interactions or might be shifted to salt concentrations beyond those investigated in this study. This finding suggests that there may be a competition between osmotic and excluded volume effects that favor swelling of the coacervate phase and that increases in the hydrophobicity of

the coacervate environment the can resist further swelling by excluding water and/or facilitating more efficient packing of polymer and dye molecules. We expect that the presence of dye could alter the location of the phase boundaries for coacervation as a consequence of these effects. However, specific quantification of the two-phase region is beyond the scope of this study.

**3.4. Electrospinning BBG- and FG-Containing PEC Fibers.** We previously demonstrated that dye-free complex coacervates could be electrospun into polyelectrolyte complex (PEC) fibers (Figure 7 and Figure S2).<sup>24</sup> This effort highlighted the importance of harnessing knowledge of coacervate phase behavior, such as the interplay between polymer and salt concentration, to achieve successful electrospinning outcomes. Here, our goal was to enable the direct electrospinning of cargo-containing PEC fibers. Thus, we sought to understand how dye-induced changes in coacervate phase behavior would affect electrospinning and the subsequent fiber formation and fiber morphology.

We were able to successfully electrospin PEC fibers containing a wide range of dye concentrations using a single-spinneret electrospinning setup. It should be noted that the electrospinning apparatus conditions used in this study were

consistent across all samples. A consistent flow rate (1 mL/h), needle orifice diameter (22 gauge), applied voltage (14 kV), spinneret-to-collector distance (20 cm), and temperature/relative humidity in the electrospinning chamber were used throughout all coacervate samples, such that variations in the fiber diameter distributions should be dominated by differences in the coacervate precursor solutions rather than the processing method. Notably, for coacervates made with 10 and 15 mM total FG concentration, it was necessary to increase the flow rate to 1.25 mL/h and the voltage to 18 and 22 kV to observe the onset of fiber formation.

While dye-free PEC fiber mats were white due to the scattering of light, fibers electrospun from BBG- and FGcontaining PSS/PDADMAC coacervates were uniformly blue and green, respectively (Figure 7a,b). SEM micrographs showed that the fibers have a continuous, cylindrical morphology, with the fiber surface decorated by salt crystals (Figure 7c), consistent with our previous work.<sup>24</sup> The presence of dye within the electrospun fibers was also confirmed via FTIR (Figure S3). It is particularly noteworthy that while salt was observed to crystallize out on the surface of the fibers, the dye was retained in the polymer matrix. Furthermore, we observed that encapsulated BBG remained in the fibers upon contact with Milli-Q water, while a small amount of FG leached. These results were consistent with the types of attractive or repulsive interactions observed previously between the two dyes and PSS in the coacervate phase. However, the as-spun fibers retain their morphology after submersion in water, regardless of cargo identity.

Next we examined the effect of increasing the concentration of BBG and FG on fiber formation. Increasing the concentration of BBG in the coacervate precursor solutions from 5 to 15 mM resulted in a mild increase in the coacervate volume from 39% of the total to 43% (Figure 3b). This slight swelling of the coacervate corresponded to a slight narrowing and shifting of the distribution of fiber diameters to smaller values with increasing BBG concentration (Figure 7d). In contrast, FG resulted in much more significant swelling of the coacervate over the same range of concentrations (42-60% volume fraction, Figure 3b). Thus, we hypothesized that the more swollen FG-containing coacervates would result in smaller diameter electrospun fibers because of their lower polymer concentrations. Our data support this hypothesis, with samples prepared from 5 mM FG resulting in significantly smaller and more monodisperse distribution of fiber diameters than for the case of BBG (Figure 7c,d). Further increases in the FG concentration resulted in even smaller diameter fibers with a discontinuous morphology (Figure 7c).<sup>7,61-64</sup>

We also examined the effect of salt on electrospinnability, examining complex coacervates prepared at 1.4-1.7 M KBr in the presence of 5 mM BBG or FG (Figure 8). Consistent with our previous results, <sup>24</sup> coacervates prepared at 1.4 M KBr were too viscous to extrude through the spinneret, even in the presence of dye. In contrast, while dye-free coacervates prepared at 1.7 M KBr formed smooth, continuous PEC fibers that were  $\sim 1.5 \, \mu \mathrm{m}$  in diameter, <sup>24</sup> the addition of 5 mM BBG or FG altered the character of the coacervate phases such that fibers could not be electrospun using the conditions tested in this study. Thus, our analysis focused on comparing samples prepared at 1.5 and 1.6 M KBr.

As expected, increasing salt concentration led to a narrower distribution of smaller diameter fibers for dye-free samples (Figure 8 and Table S4).<sup>24</sup> On average, the dye-free fiber

diameters were 4.04  $\pm$  1.00 and 1.59  $\pm$  0.45  $\mu m$  for salt concentrations of 1.5 and 1.6 M KBr, respectively. This decrease in fiber diameter was even more dramatic for FG-containing samples, which shifted from a broad distribution of diameters centered around 4.51  $\pm$  1.28  $\mu m$  at 1.5 M KBr to a significantly smaller and narrower distribution around 0.73  $\pm$  0.12  $\mu m$  for 1.6 M KBr. Surprisingly, we observed very little change in the distribution of fiber diameters for BBG-containing fiber mats, despite significant differences in the volume of the coacervate phase at the two different salt concentrations (Figure 6d,e). We hypothesize that the attractive interactions between BBG and PSS may help to counterbalance salt-induced changes in the rheological properties of the coacervates associated with swelling.

While we were able to successfully electrospin smooth, continuous BBG-containing PEC fibers at all salt and dye conditions tested, FG-containing samples were much more sensitive to the combination of dye and salt concentration. At 1.6 M KBr we observed a discontinuous morphology above 5 mM dye (Figure 7c). This contrasts the results obtained at 1.5 M KBr, where smooth, continuous FG-containing PEC fibers were obtained over the range of dye concentrations examined (Figure S4e,f). These results highlight the importance of understanding how the presence of cargo affects the overall coacervate phase behavior and how parameters such as salt and cargo concentration can be tuned to facilitate fiber formation.

**3.5. Electrospinning Fluorescein- and Rhodamine-Containing PEC Fibers.** Building on our observations with BBG and FG, we examined how the subtle structural variations between F123, R6G, RB, and FS would affect electrospinnability. Despite their smaller size, all four of these dyes caused significantly more swelling of the coacervate phase than either BBG or FG (Figure 6d,e), and as was the case with BBG and FG, the magnitude of swelling induced by the presence of the dye did not necessarily correlate with spinnability and/or fiber diameter.

The results for FS-containing coacervates were similar to those reported for coacervates containing FG. At 1.5 M KBr, both FS and FG formed large diameter fibers with a broad distribution of diameters, as was also observed for the dye-free case (Figure 9c and Figure S4f). Furthermore, the average diameter of these broad size distributions was correlated to the degree of coacervate swelling (Figure 6d,e). Increasing the salt concentration to 1.6 M KBr resulted in a significantly narrower distribution of smaller diameter fibers (Figure S5e). Thus, we hypothesized that in the absence of attractive interactions between the cargo and the polymers of the coacervates the size of the resulting fibers will be dominated by the rheological character of the swollen coacervate phase.

For the rhodamine dyes, as with FS, we were able to successfully electrospin smooth, cylindrical, and uniformly colored fibers at a salt concentration of 1.5 M KBr (Figure 9). However, at a salt concentration of 1.6 M KBr, we only observed the formation of smooth, continuous fibers for R123 and FS (Figure S5). R6G- and RB-containing samples showed a discontinuous morphology suggesting beading and potentially, the onset of fiber formation (Figure S5g). If one only considered the attractive interactions between dye molecules and PSS as a criterion for electrospinnability, then the results from 1.6 M KBr might be unexpected. However, the attractive dye—polymer interactions that might help to resist changes in the rheological character of the coacervate were counterbalanced by the significant swelling observed for these dyes

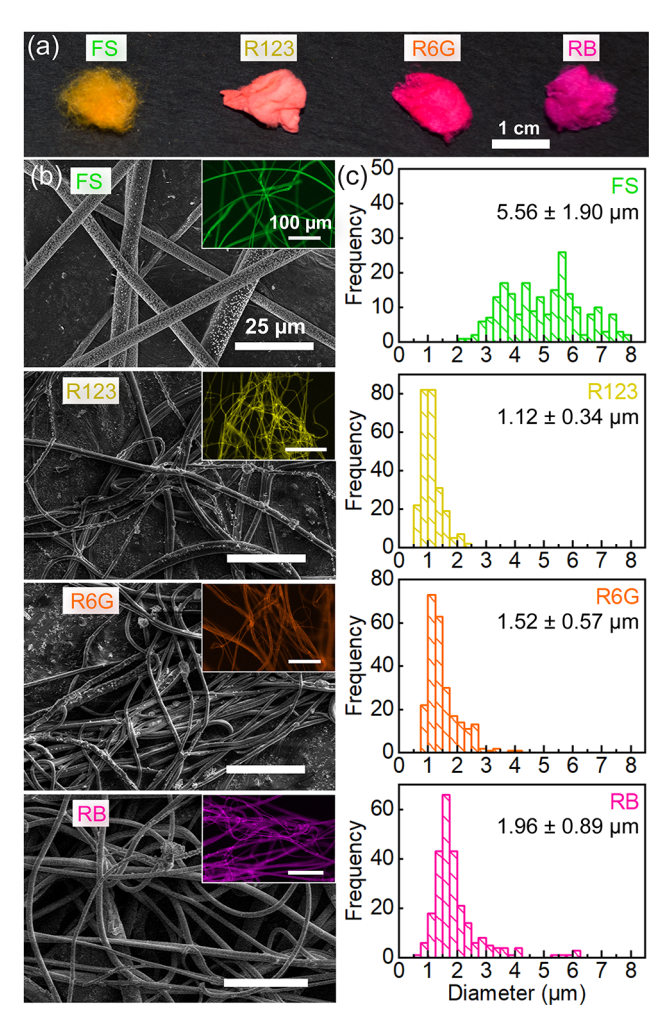


**Figure 9.** (a) Digital photographs, (b) SEM and (inset) fluorescence micrographs, and (c) fiber diameter distributions of PSS/PDADMAC PEC fibers containing FS, R123, R6G, and RB. (c) The average fiber diameter and standard deviation are indicated, n = 250. All fibers were electrospun from 0.5 M PSS/PDADMAC, on a monomer basis, in 1.5 M KBr with 5 mM of total dye. Electrospinning conditions used were 1 mL/h, 14 kV, and 20 cm.

(Figure 6d,e and Figure S5d). For example, R6G and RB showed significantly more swelling at 1.6 M KBr than any of the other dyes, potentially accounting for the observed difficulties in fiber formation. Interestingly, R123 was the only rhodamine/fluorescein dye that completely resisted leaching upon submersion in Milli-Q water, further supporting the idea of strong polymer—dye interactions.

In summary, our results suggest that for successful electrospinning it is critical to understand how cargo molecules interact with components of the coacervate matrix and how cargo molecules alter the overall coacervate phase behavior. While a detailed characterization of the rheological properties of coacervate precursor solutions is beyond the scope of this study, our results suggest that for a given coacervate system there is a critical polymer concentration (or degree of swelling) beyond which electrospinning cannot be realized. Furthermore, the location of this critical point can be shifted based on whether the encapsulated cargo molecules participate in attractive interactions with the coacervate matrix.

# 4. CONCLUSIONS

We report the first demonstration of electrospun, cargocontaining PEC fibers from aqueous complex coacervates, using a model system of PSS and PDADMAC. Six fluorescent dyes were used to probe the effect of variations in cargo hydrophobicity, structure, and charge on the resulting uptake into complex coacervates for subsequent use in electrospinning. While preferential partitioning into the coacervate phase was observed for all of the model compounds used in this study, the presence of attractive interactions between dye molecules and at least one of the polymer molecules significantly increased the level of partitioning observed. Furthermore, we observed a complex interplay in terms of how salt and dye concentrations can be used to tune the phase behavior of the complex coacervates to modulate both dye encapsulation and subsequent fiber formation and morphology. The use of aqueous complex coacervation as a strategy to enable the green processing of PEC fibers has significant potential for use in applications related to biomedicine, energy, and environmental remediation where cargo-loaded fibers are

# ASSOCIATED CONTENT

# **S** Supporting Information

The Supporting Information is available free of charge on the ACS Publications website at DOI: 10.1021/acs.macromol.8b01709.

Tabulated information about the molecular characteristics of the dyes, peak absorbance wavelengths as a function of solution conditions, and dye partition coefficients; plots of the ratio of the number of PSS/PDADMAC monomers per dye molecule present in the coacervate for BBG and FG as a function of salt and dye concentration; SEM micrograph of dye-free PEC fibers; FTIR characterization; tabulated data on the average fiber diameter as a function of dye and salt concentration; additional data on dye encapsulation and subsequent fiber formation at different salt concentrations (PDF)

# AUTHOR INFORMATION

### **Corresponding Authors**

\*E-mail perrys@engin.umass.edu.

\*E-mail schiffman@ecs.umass.edu.

#### ORCID ®

Jessica D. Schiffman: 0000-0002-1265-5392 Sarah L. Perry: 0000-0003-2301-6710

#### Notes

The authors declare no competing financial interest.

### ACKNOWLEDGMENTS

We acknowledge Rasmia R. Shamsi, Ruoting Wang, and Bryan M. Chua for their preliminary experiments. We thank Prof. Alexander Ayzner for helpful discussions. X.M. acknowledges the support of the National Science Foundation NRT-SMLS program (DGE-1545399). We acknowledge the support of the National Science Foundation (NSF CMMI-1727660) and a UMass Amherst Faculty Research Grant. We acknowledge the facilities at the W.M. Keck Center for Electron Microscopy.

# REFERENCES

- (1) Ramakrishna, S.; Fujihara, K.; Teo, W.-E.; Lim, T.-C.; Ma, Z. An Introduction to Electrospinning and Nanofibers; World Scientific Publishing Co. Pte. Ltd.: 2005.
- (2) Ramakrishna, S.; Fujihara, K.; Teo, W.-E.; Yong, T.; Ma, Z.; Ramaseshan, R. Electrospun Nanofibers: Solving Global Issues. *Mater. Today* **2006**, *9*, 40–50.
- (3) Mittal, V. Use of Electrospinning for Encapsulation. In *Encapsulation Nanotechnologies*; Pérez-Mariá, R., Fabra, M. J., Lagarón, J. M., López-Rubio, A., Eds.; John Wiley & Sons, Inc.: Hoboken, NJ, 2013; Vol. 16, pp 190–237.
- (4) Rieger, K. A.; Birch, N. P.; Schiffman, J. D. Designing Electrospun Nanofiber Mats to Promote Wound Healing A Review. J. Mater. Chem. B 2013, 1, 4531–4541.
- (5) Sridhar, R.; Sundarrajan, S.; Vanangamudi, A.; Singh, G.; Matsuura, T.; Ramakrishna, S. Green Processing Mediated Novel Polyelectrolyte Nanofibers and Their Antimicrobial Evaluation. *Macromol. Mater. Eng.* **2014**, 299, 283–289.
- (6) Engel, Y.; Schiffman, J. D.; Goddard, J. M.; Rotello, V. M. Nanomanufacturing of Biomaterials. *Mater. Today* **2012**, *15*, 478–485.
- (7) Ignatova, M.; Manolova, N.; Rashkov, I. Electrospun Antibacterial Chitosan-Based Fibers. *Macromol. Biosci.* **2013**, *13*, 860–872.
- (8) Pham, Q. P.; Sharma, U.; Mikos, A. G. Electrospinning of Polymeric Nanofibers for Tissue Engineering Applications: a Review. *Tissue Eng.* **2006**, *12*, 1197–1264.
- (9) Ignatova, M. G.; Manolova, N. E.; Rashkov, I. B.; Markova, N. D.; Toshkova, R. A.; Georgieva, A. K.; Nikolova, E. B. Poly(3-Hydroxybutyrate)/Caffeic Acid Electrospun Fibrous Materials Coated with Polyelectrolyte Complex and Their Antibacterial Activity and In Vitro Antitumor Effect Against HeLa Cells. *Mater. Sci. Eng., C* 2016, 65, 379–392.
- (10) Son, Y. J.; Kim, W. J.; Yoo, H. S. Therapeutic Applications of Electrospun Nanofibers for Drug Delivery Systems. *Arch. Pharmacal Res.* **2014**, *37*, 69–78.
- (11) Chunder, A.; Sarkar, S.; Yu, Y.; Zhai, L. Fabrication of Ultrathin Polyelectrolyte Fibers and Their Controlled Release Properties. *Colloids Surf., B* **2007**, *58*, 172–179.
- (12) Wen, P.; Zong, M.-H.; Linhardt, R. J.; Feng, K.; Wu, H. Electrospinning: a Novel Nano-Encapsulation Approach for Bioactive Compounds. *Trends Food Sci. Technol.* **2017**, *70*, 56–68.
- (13) Wang, C.; Yan, K.-W.; Lin, Y.-D.; Hsieh, P. C. H. Biodegradable Core/Shell Fibers by Coaxial Electrospinning: Processing, Fiber Characterization, and Its Application in Sustained Drug Release. *Macromolecules* **2010**, *43*, 6389–6397.
- (14) Kumar, A. Core-Shell Nanofibers: Nano Channel and Capsule by Coaxial Electrospinning. In *Nanofibers*; Li, F.; Zhao, Y.; Song, Y., Eds.; 2018; pp 419–438.
- (15) Tiwari, S. K.; Venkatraman, S. S. Importance of Viscosity Parameters in Electrospinning: of Monolithic and Core—Shell Fibers. *Mater. Sci. Eng., C* **2012**, 32, 1037—1042.
- (16) Qi, H.; Hu, P.; Xu, J.; Wang, A. Encapsulation of Drug Reservoirs in Fibers by Emulsion Electrospinning: Morphology Characterization and Preliminary Release Assessment. *Biomacromolecules* **2006**, *7*, 2327–2330.
- (17) Maleki, M.; Latifi, M.; Amani-Tehran, M.; Mathur, S. Electrospun Core-Shell Nanofibers for Drug Encapsulation and Sustained Release. *Polym. Eng. Sci.* **2013**, *53*, 1770–1779.
- (18) Garrett, D. E. Manufacturing Cost. In *Chemical Engineering Economics*; Garrett, D. E., Ed.; Springer: Dordrecht, 1989; pp 44-46.
- (19) Luo, D.; Zhang, X.; Shahid, S.; Cattell, M. J.; Gould, D. J.; Sukhorukov, G. B. Electrospun Poly(Lactic Acid) Fibers Containing Novel Chlorhexidine Particles with Sustained Antibacterial Activity. *Biomater. Sci.* **2017**, *5*, 111–119.
- (20) García-Moreno, P. J.; Stephansen, K.; van der Kruijs, J.; Guadix, A.; Guadix, E. M.; Chronakis, I. S.; Jacobsen, C. Encapsulation of Fish Oil in Nanofibers by Emulsion Electrospinning: Physical Characterization and Oxidative Stability. *J. Food Eng.* **2016**, *183*, 39–49.

- (21) Liao, Y.; Zhang, L.; Gao, Y.; Zhu, Z.-T.; Fong, H. Preparation, Characterization, and Encapsulation/Release Studies of a Composite Nanofiber Mat Electrospun from an Emulsion Containing Poly-(Lactic-Co-Glycolic Acid). *Polymer* **2008**, *49*, 5294–5299.
- (22) Chou, S.-F.; Carson, D.; Woodrow, K. A. Current Strategies for Sustaining Drug Release from Electrospun Nanofibers. *J. Controlled Release* **2015**, 220, 584–591.
- (23) Boas, M.; Gradys, A.; Vasilyev, G.; Burman, M.; Zussman, E. Electrospinning Polyelectrolyte Complexes: pH-Responsive Fibers. *Soft Matter* **2015**, *11*, 1739–1747.
- (24) Meng, X.; Perry, S. L.; Schiffman, J. D. Complex Coacervation: Chemically Stable Fibers Electrospun from Aqueous Polyelectrolyte Solutions. *ACS Macro Lett.* **2017**, *6*, 505–511.
- (25) Colby, R. H. Structure and Linear Viscoelasticity of Flexible Polymer Solutions: Comparison of Polyelectrolyte and Neutral Polymer Solutions. *Rheol. Acta* **2010**, *49*, 425–442.
- (26) Spruijt, E.; Westphal, A. H.; Borst, J. W.; Cohen Stuart, M. A.; van der Gucht, J. Binodal Compositions of Polyelectrolyte Complexes. *Macromolecules* **2010**, *43*, 6476–6484.
- (27) Chollakup, R.; Beck, J. B.; Dirnberger, K.; Tirrell, M.; Eisenbach, C. D. Polyelectrolyte Molecular Weight and Salt Effects on the Phase Behavior and Coacervation of Aqueous Solutions of Poly(Acrylic Acid) Sodium Salt and Poly(Allylamine) Hydrochloride. *Macromolecules* **2013**, *46*, 2376–2390.
- (28) van der Gucht, J.; Spruijt, E.; Lemmers, M.; Cohen Stuart, M. A. Polyelectrolyte Complexes: Bulk Phases and Colloidal Systems. *J. Colloid Interface Sci.* **2011**, *361*, 407–422.
- (29) Wang, Q.; Schlenoff, J. B. The Polyelectrolyte Complex/Coacervate Continuum. *Macromolecules* **2014**, 47, 3108–3116.
- (30) Perry, S. L.; Li, Y.; Priftis, D.; Leon, L.; Tirrell, M. The Effect of Salt on the Complex Coacervation of Vinyl Polyelectrolytes. *Polymers* **2014**, *6*, 1756–1772.
- (31) de Kruif, C. G.; Weinbreck, F.; de Vries, R. Complex Coacervation of Proteins and Anionic Polysaccharides. *Curr. Opin. Colloid Interface Sci.* **2004**, *9*, 340–349.
- (32) Kayitmazer, A. B.; Seeman, D.; Minsky, B. B.; Dubin, P. L.; Xu, Y. Protein—Polyelectrolyte Interactions. *Soft Matter* **2013**, *9*, 2553—2583.
- (33) Priftis, D.; Tirrell, M. Phase Behaviour and Complex Coacervation of Aqueous Polypeptide Solutions. *Soft Matter* **2012**, *8*, 9396–9405.
- (34) Perry, S. L.; Leon, L.; Hoffmann, K. Q.; Kade, M. J.; Priftis, D.; Black, K. A.; Wong, D.; Klein, R. A.; Pierce, C. F., III; Margossian, K. O.; Whitmer, J. K.; Qin, J.; de Pablo, J. J.; Tirrell, M. Chirality-Selected Phase Behaviour in Ionic Polypeptide Complexes. *Nat. Commun.* **2015**, *6*, 6052.
- (35) Black, K. A.; Priftis, D.; Perry, S. L.; Yip, J.; Byun, W. Y.; Tirrell, M. Protein Encapsulation via Polypeptide Complex Coacervation. *ACS Macro Lett.* **2014**, *3*, 1088–1091.
- (36) Nolles, A.; van Dongen, N. J. E.; Westphal, A. H.; Visser, A. J. W. G.; Kleijn, J. M.; van Berkel, W. J. H.; Borst, J. W. Encapsulation into Complex Coacervate Core Micelles Promotes EGFP Dimerization. *Phys. Chem. Chem. Phys.* **2017**, *19*, 11380–11389.
- (37) Madene, A.; Jacquot, M.; Scher, J.; Desobry, S. Flavour Encapsulation and Controlled Release A Review. *Int. J. Food Sci. Technol.* **2006**, *41*, 1–21.
- (38) Moran, D. P. J.; Halstead, P. W.; Co, L. B. Food Product, U.S. Patent 4,305,964. December 15, 1981.
- (39) Katayose, S.; Kataoka, K. Water-Soluble Polyion Complex Associates of DNA and Poly(Ethylene Glycol)—Poly(L-Lysine) Block Copolymer. *Bioconjugate Chem.* **1997**, *8*, 702—707.
- (40) Oishi, M.; Nagasaki, Y.; Itaka, K.; Nishiyama, N.; Kataoka, K. Lactosylated Poly(Ethylene Glycol)-siRNA Conjugate Through Acid-Labile B-Thiopropionate Linkage to Construct pH-Sensitive Polyion Complex Micelles Achieving Enhanced Gene Silencing in Hepatoma Cells. J. Am. Chem. Soc. 2005, 127, 1624–1625.
- (41) Johnson, N. R.; Wang, Y. Coacervate Delivery Systems for Proteins and Small Molecule Drugs. *Expert Opin. Drug Delivery* **2014**, *11*, 1829–1832.

(42) Chu, H.; Johnson, N. R.; Mason, N. S.; Wang, Y. A [Polycation:Heparin] Complex Releases Growth Factors with Enhanced Bioactivity. *J. Controlled Release* **2011**, *150*, 157–163.

- (43) Johnson, N. R.; Kruger, M.; Goetsch, K. P.; Zilla, P.; Bezuidenhout, D.; Wang, Y.; Davies, N. H. Coacervate Delivery of Growth Factors Combined with a Degradable Hydrogel Preserves Heart Function After Myocardial Infarction. ACS Biomater. Sci. Eng. 2015, 1, 753–759.
- (44) Turovsky, T.; Khalfin, R.; Kababya, S.; Schmidt, A.; Barenholz, Y.; Danino, D. Celecoxib Encapsulation in B-Casein Micelles: Structure, Interactions, and Conformation. *Langmuir* **2015**, *31*, 7183–7192.
- (45) Rutz, J. K.; Borges, C. D.; Zambiazi, R. C.; Crizel-Cardozo, M. M.; Kuck, L. S.; Noreña, C. P. Z. Microencapsulation of Palm Oil by Complex Coacervation for Application in Food Systems. *Food Chem.* **2017**, 220, 59–66.
- (46) Tiwari, A.; Bindal, S.; Bohidar, H. B. Kinetics of Protein—Protein Complex Coacervation and Biphasic Release of Salbutamol Sulfate from Coacervate Matrix. *Biomacromolecules* **2009**, *10*, 184—180
- (47) Zhao, M.; Zacharia, N. S. Sequestration of Methylene Blue Into Polyelectrolyte Complex Coacervates. *Macromol. Rapid Commun.* **2016**, 37, 1249–1255.
- (48) Zhao, M.; Eghtesadi, S. A.; Dawadi, M. B.; Wang, C.; Huang, S.; Seymore, A. E.; Vogt, B. D.; Modarelli, D. A.; Liu, T.; Zacharia, N. S. Partitioning of Small Molecules in Hydrogen-Bonding Complex Coacervates of Poly(Acrylic Acid) and Poly(Ethylene Glycol) or Pluronic Block Copolymer. *Macromolecules* 2017, 50, 3818–3830.
- (49) Huang, S.; Zhao, M.; Dawadi, M. B.; Cai, Y.; Lapitsky, Y.; Modarelli, D. A.; Zacharia, N. S. Effect of Small Molecules on the Phase Behavior and Coacervation of Aqueous Solutions of Poly(Diallyldimethylammonium Chloride) and Poly(Sodium 4-Styrene Sulfonate). J. Colloid Interface Sci. 2018, 518, 216–224.
- (50) Liu, Y.; Momani, B.; Winter, H. H.; Perry, S. L. Rheological Characterization of Liquid-to-Solid Transitions in Bulk Polyelectrolyte Complexes. *Soft Matter* **2017**, *13*, 7332–7340.
- (51) Rieger, K. A.; Thyagarajan, R.; Hoen, M. E.; Yeung, H. F.; Ford, D. M.; Schiffman, J. D. Transport of Microorganisms Into Cellulose Nanofiber Mats. RSC Adv. 2016, 6, 24438–24445.
- (52) Lv, K.; Perriman, A. W.; Mann, S. Photocatalytic Multiphase Micro-Droplet Reactors Based on Complex Coacervation. *Chem. Commun.* **2015**, *51*, 8600–8602.
- (53) Perry, S. L.; Sing, C. E. PRISM-Based Theory of Complex Coacervation: Excluded Volume Versus Chain Correlation. *Macromolecules* **2015**, *48*, 5040–5053.
- (54) Radhakrishna, M.; Basu, K.; Liu, Y.; Shamsi, R.; Perry, S. L.; Sing, C. E. Molecular Connectivity and Correlation Effects on Polymer Coacervation. *Macromolecules* **2017**, *50*, 3030–3037.
- (55) Lytle, T. K.; Sing, C. E. Transfer Matrix Theory of Polymer Complex Coacervation. *Soft Matter* **2017**, *13*, 7001–7012.
- (56) Lytle, T. K.; Sing, C. E. Tuning Chain Interaction Entropy in Complex Coacervation Using Polymer Stiffness, Architecture, and Salt Valency. *Mol. Syst. Des. Eng.* **2018**, *3*, 183–196.
- (57) Salehi, A.; Larson, R. G. A Molecular Thermodynamic Model of Complexation in Mixtures of Oppositely Charged Polyelectrolytes with Explicit Account of Charge Association/Dissociation. *Macromolecules* **2016**, *49*, 9706–9719.
- (58) Salehi, A.; Desai, P. S.; Li, J.; Steele, C. A.; Larson, R. G. Relationship Between Polyelectrolyte Bulk Complexation and Kinetics of Their Layer-by-Layer Assembly. *Macromolecules* **2015**, 48, 400–409.
- (59) Li, L.; Srivastava, S.; Andreev, M.; Marciel, A. B.; de Pablo, J. J.; Tirrell, M. V. Phase Behavior and Salt Partitioning in Polyelectrolyte Complex Coacervates. *Macromolecules* **2018**, *51*, 2988–2995.
- (60) Porcel, C. H.; Schlenoff, J. B. Compact Polyelectrolyte Complexes: "Saloplastic" Candidates for Biomaterials. *Biomacromolecules* **2009**, *10*, 2968–2975.
- (61) Mit-Uppatham, C.; Nithitanakul, M.; Supaphol, P. Ultrafine Electrospun Polyamide-6 Fibers: Effect of Solution Conditions on

Morphology and Average Fiber Diameter. *Macromol. Chem. Phys.* **2004**, 205, 2327–2338.

- (62) Schiffman, J. D.; Schauer, C. L. A Review: Electrospinning of Biopolymer Nanofibers and Their Applications. *Polym. Rev.* **2008**, *48*, 317–352.
- (63) Davidov-Pardo, G.; Joye, I. J.; McClements, D. J. Adv. Protein Chem. Struct. Biol. 2015, 98, 293-325.
- (64) Rutledge, G. C.; Fridrikh, S. V. Formation of Fibers by Electrospinning. *Adv. Drug Delivery Rev.* **2007**, *59*, 1384–1391.